

Phase modulation atomic force microscope with true atomic resolution

Takeshi Fukuma,^{a)} Jason I. Kilpatrick, and Suzanne P. Jarvis
*Centre for Research on Adaptive Nanostructures and Nanodevices, Lincoln Place Gate,
 Trinity College Dublin, Dublin 2, Ireland*

(Received 6 May 2006; accepted 13 November 2006; published online 21 December 2006)

We have developed a dynamic force microscope (DFM) working in a novel operation mode which is referred to as phase modulation atomic force microscopy (PM-AFM). PM-AFM utilizes a fixed-frequency excitation signal to drive a cantilever, which ensures stable imaging even with occasional tip crash and adhesion to the surface. The tip-sample interaction force is detected as a change of the phase difference between the cantilever deflection and excitation signals and hence the time response is not influenced by the Q factor of the cantilever. These features make PM-AFM more suitable for high-speed imaging than existing DFM techniques such as amplitude modulation and frequency modulation atomic force microscopies. Here we present the basic principle of PM-AFM and the theoretical limit of its performance. The design of the developed PM-AFM is described and its theoretically limited noise performance is demonstrated. Finally, we demonstrate the true atomic resolution imaging capability of the developed PM-AFM by imaging atomic-scale features of mica in water. © 2006 American Institute of Physics. [DOI: 10.1063/1.2405361]

I. INTRODUCTION

Dynamic force microscopy¹ (DFM) has been used for various applications due to its high spatial resolution and high force sensitivity. There have been two major operation modes in DFM, which are referred to as amplitude modulation¹ and frequency modulation² atomic force microscopies (AM- and FM-AFMs). Although the theoretically predicted minimum detectable force, that is limited by the thermal Brownian motion of the cantilever, is almost the same for both operation modes,^{1,2} they have distinguishing characteristics due to the difference in the cantilever excitation and force detection methods.

In AM-AFM, a cantilever is driven by an ac excitation signal with fixed amplitude (A_{exc}) and frequency around the cantilever resonance. This cantilever excitation method is hereafter referred to as external excitation. The tip-sample interaction force (F_{ts}) is detected as a shift (ΔA) of the cantilever oscillation amplitude (A). The external excitation enables stable imaging of rough or dynamically changing surfaces where the occasional tip crash and adhesion are often hard to avoid.³⁻⁵ However, ΔA is influenced by both conservative and dissipative interaction forces, which can lead to topographic artifacts in the obtained AFM images. In addition, the time response of ΔA becomes slower with increasing Q factor. This prohibits the use of AM-AFM in vacuum and limits the imaging speed in air.

In FM-AFM, a cantilever is always driven at resonance using a self-excitation circuit. F_{ts} is detected as a shift (Δf) of the resonance frequency. In contrast to ΔA , the time response of Δf is not influenced by the Q factor. Thus, FM-AFM can operate in vacuum and exhibit extremely high force sensitivity and spatial resolution owing to the high Q

factor.^{6,7} In addition, FM-AFM operating in constant amplitude mode is capable of measuring the conservative and dissipative interaction forces independently.⁸⁻¹² Therefore, a variation in dissipative interaction force does not cause topographic artifacts in FM-AFM. However, a stable self-excitation requires a clean cantilever deflection signal and, hence, can be disrupted by the occasional tip crash or adhesion. Practically, this often limits the maximum imaging speed in FM-AFM.

In this study, we have developed a DFM working in a novel operation mode which is referred to as phase modulation atomic force microscopy (PM-AFM). In PM-AFM, a cantilever is oscillated in external-excitation mode at the cantilever resonance frequency (f_0), this ensures stable imaging even with the occasional tip crash or adhesion to the surface. F_{ts} is detected as a change ($\Delta\phi$) of the phase difference between the cantilever deflection and excitation signals and, hence, the time response is not influenced by the Q factor. These features make PM-AFM more suitable for high-speed imaging than AM- and FM-AFM. Here we present the basic principle of PM-AFM and the theoretical limit of its performance. The design of the developed PM-AFM is described and its theoretically limited noise performance is demonstrated. Finally, we demonstrate the true atomic resolution imaging capability of the developed PM-AFM by imaging atomic-scale features of mica in water.

II. BASIC PRINCIPLES OF PM-AFM

A. Phase shift

The equation of motion for a cantilever driven by an external-excitation is given by

^{a)}Electronic mail: takeshi.fukuma@tcd.ie

$$\frac{d^2z}{dt^2} + \frac{\omega_0}{Q} \frac{dz}{dt} + \omega_0^2 z = \omega_0^2 A_{\text{exc}} \cos(\omega_0 t) + \frac{\omega_0^2}{k} F_{\text{ts}}, \quad (1)$$

where $\omega_0 (\equiv 2\pi f_0)$, z , and k are angular velocity of cantilever oscillation, vertical tip position, and spring constant of the cantilever, respectively.

Assuming harmonic oscillation of the cantilever, z is given by

$$z = A \sin(\omega_0 t + \Delta\varphi), \quad (2)$$

where $\Delta\varphi$ is defined as the phase shift of the cantilever oscillation with respect to a 90° delay from the phase of cantilever excitation signal.

Fourier coefficients of the ω_0 components of F_{ts} are given by

$$F_c = \frac{\omega_0}{\pi} \int_0^{2\pi/\omega_0} F_{\text{ts}} \sin(\omega_0 t + \Delta\varphi) dt, \quad (3)$$

$$F_d = \frac{\omega_0}{\pi} \int_0^{2\pi/\omega_0} F_{\text{ts}} \cos(\omega_0 t + \Delta\varphi) dt. \quad (4)$$

F_c represents the magnitude of ω_0 components with the same phase as that of z , which is referred to as conservative force. On the other hand, F_d represents the magnitude of the ω_0 components of which the phase is 90° delayed from that of z and, hence, is referred to as dissipative force.

Since we assumed harmonic oscillation of the cantilever by Eq. (2), here we consider only ω_0 components of F_{ts} as described by

$$F_{\text{ts}} = F_c \sin(\omega_0 t + \Delta\varphi) + F_d \cos(\omega_0 t + \Delta\varphi). \quad (5)$$

From Eqs. (1), (2), and (5) and $|\Delta\varphi| \ll 1$, $\Delta\varphi$, and ΔA are given by

$$\Delta\varphi = -\frac{Q}{kA_0} F_c, \quad (6)$$

$$\Delta A = \frac{Q}{k} F_d - \frac{Q^2}{k^2 A_0} F_c^2, \quad (7)$$

where $A_0 (=QA_{\text{exc}})$ is the value of A when $F_{\text{ts}}=0$. Equation (7) shows both F_c and F_d influence ΔA . In addition, the change in ΔA results in a change of the tip-sample separation, which in turn varies F_c . Eventually, both of F_c and F_d influence ΔA and $\Delta\varphi$.

It is possible to operate PM-AFM in constant amplitude mode, where A is maintained constant by controlling A_{exc} using an automatic gain control circuit. In this case, $\Delta\varphi$ and the shift of A_{exc} (ΔA_{exc}) are given by

$$\Delta\varphi = -\frac{F_c}{kA_{\text{exc}0} - F_d}, \quad (8)$$

$$\Delta A_{\text{exc}} = -\frac{1}{k} F_d + \frac{F_c^2}{k(kA_{\text{exc}0} - F_d)}, \quad (9)$$

where $A_{\text{exc}0}$ is a value for A_{exc} when $F_{\text{ts}}=0$. These equations show that both F_c and F_d influence $\Delta\varphi$ and ΔA_{exc} even in constant amplitude mode. Thus, conservative and dissipative forces cannot be measured separately in PM-AFM.

B. Phase noise

When $\Delta\varphi$ is modulated at a frequency f_m by F_{ts} , this gives rise to a power spectral peaks at $f_0 \pm f_m$ in the frequency spectrum of cantilever deflection signal. These frequency components are converted to f_m component of phase signal as they are demodulated by a PM detector such as a lock-in amplifier. Similarly, deflection noise at $f_0 \pm f_m$ is converted to phase noise at f_m in the phase signal. Therefore, if F_{ts} is measure with a bandwidth B , the deflection noise densities integrated over the frequency range from $f_0 - B$ to $f_0 + B$ will contribute to the noise in the demodulated phase signal.

The noise in the cantilever deflection signal is comprised of two major components: noise arising from the cantilever deflection sensor and that from the thermal Brownian motion of the cantilever itself. Recent studies^{13,14} have shown that the spectral density of the noise arising from the deflection sensor (n_{zs}) can be reduced to less than that from cantilever thermal Brownian motion (n_{zB}) for f_m values less than practical B (typically less than 1 kHz). Thus, we mainly consider the contribution of n_{zB} to the phase noise in the rest of the discussion. n_{zB} at a frequency f is given by

$$n_{zB} = \sqrt{\frac{2k_B T}{\pi f_0 k Q} \frac{1}{[1 - (f/f_0)^2]^2 + [f/(f_0 Q)]^2}}, \quad (10)$$

where k_B and T are Boltzmann constant and absolute temperature, respectively.

Assuming $f_m \ll f_0$ and the thermal vibration of the cantilever is much smaller than A , the phase noise density n_p at a frequency $f=f_0+f_m$ is given by

$$n_p = \sqrt{\frac{4k_B T}{\pi f_0 k Q A^2} \frac{1}{4(f_m/f_0)^2 + 1/Q^2}}. \quad (11)$$

For low- Q environments (e.g., in liquid) where $Q \ll f_0/(2B)$, phase noise density n_{pL} and total phase noise $\delta\varphi_L$ are approximated as

$$n_{pL} = \sqrt{\frac{4k_B T Q}{\pi f_0 k A^2}}, \quad (12)$$

$$\delta\varphi_L = \sqrt{\frac{4k_B T Q B}{\pi f_0 k A^2}}. \quad (13)$$

These equations show that the phase noise spectrum in liquid is flat (white noise) and, hence, the total phase noise increases in proportion to \sqrt{B} .

For high- Q environments (e.g., in vacuum) where $Q \gg f_0/(2B)$, total phase noise $\delta\varphi_H$ is approximated as

$$\delta\varphi_H = \sqrt{\frac{k_B T}{k A^2}}. \quad (14)$$

This equation shows that the phase noise in vacuum is constant regardless of B as long as the phase noise arising from the deflection sensor ($n_{zs} \sqrt{2B}/A$) is negligible compared to the noise described by Eq. (14). This is a strong advantage of PM-AFM over AM-AFM and FM-AFM for high-speed imaging.

C. Minimum detectable force

From Eqs. (6) and (13) and $\Delta A \ll A_0$, the minimum detectable force in low- Q environments (δF_L)_{PM} is given by

$$(\delta F_L)_{PM} = \sqrt{\frac{4kk_B T B}{\pi f_0 Q}}. \quad (15)$$

For typical experimental parameters in liquid ($k = 20$ N/m, $T = 297$ K, $B = 1$ kHz, $f_0 = 140$ kHz, $Q = 7$), $(\delta F_L)_{PM} = 10.3$ pN. This force resolution is much smaller than the typical load forces (50–100 pN) for high-resolution imaging of biological systems.^{15,16}

For the small amplitude approximation, the minimum detectable force gradient ($\delta F'$) is roughly given by $\delta F' = \delta F_L/A$. Thus, $\delta F'$ in PM-AFM is almost the same as that in AM-AFM.¹ As for FM-AFM, $\delta F'$ in low- Q environments has not been reported. Analysis of the frequency noise in FM-AFM when the Q factor is low is complicated by the wide spectral width of the cantilever self-oscillation. The frequency noise spectrum is influenced by the characteristics of the phase-locked loop (PLL) circuit or the bandpass (or low-pass) filter in the self-excitation circuit.¹⁷ Further analyses are required for detailed comparison with FM-AFM in low- Q environments.

The minimum detectable force in high- Q environments $(\delta F_H)_{PM}$ is obtained from Eqs. (6) and (14) in a similar manner

$$(\delta F_H)_{PM} = \sqrt{\frac{kk_B T}{Q^2}}. \quad (16)$$

The minimum detectable force for FM $(\delta F_H)_{FM}$ in high- Q environments² is exactly the same as Eq. (15) and, hence, the ratio between $(\delta F_H)_{PM}$ and $(\delta F_H)_{FM}$ is given by

$$(\delta F_H)_{PM}/(\delta F_H)_{FM} = \sqrt{\frac{\pi f_0}{4BQ}}. \quad (17)$$

This ratio is much smaller than 1 for most of the experimental conditions in vacuum due to the high Q factor. This means PM-AFM can achieve higher force resolution than FM-AFM in vacuum if the same cantilever parameters are used. This difference becomes more evident when B becomes wider and therefore PM-AFM has a strong advantage over FM-AFM for high-speed imaging in vacuum.

D. Limitations in high- Q environments

In PM-AFM, a cantilever is always driven at the fixed frequency f_0 . Thus, Δf induced by F_{ts} has to be less than the half width of the resonance peak

$$|\Delta f| \approx \frac{f_0}{2k} |F'_{ts}| < \frac{f_0}{2Q}. \quad (18)$$

Note that this condition is equivalent to $|\Delta\varphi| < 1$. Also note that Δf is not defined as driving frequency shift but as resonance frequency shift and hence is commonly used for both PM- and FM-AFM in this article.

Although this condition is easily satisfied in low- Q environments, typical operating conditions in vacuum do not satisfy this requirement. For example, typical $|\Delta f|$ for high-

resolution imaging in vacuum is 50–200 Hz (Ref. 18) while the half width of the resonance peak in vacuum is 3–30 Hz.

One of the possible solutions is to operate the distance feedback at the repulsive force branch of $\Delta\varphi$ versus distance curve and adjust the $\Delta\varphi$ setpoint to a value around the zero-cross point (this operating condition will be illustrated later in Fig. 3). In this case, it would be necessary to use a small A to avoid sample damage, which in turn requires the use of a stiff cantilever to avoid tip adhesion. This small-amplitude operation has been recently proven to increase the sensitivity to short-range interaction force and improve the spatial resolution.^{19–21} However, in the case of a stiff cantilever, the resonance peak width tends to be even narrower than that for soft cantilevers (depending on the cantilever parameters), which could make the distance feedback operation unstable especially for high-speed imaging. In that case, practical imaging speed may be limited by the stable operation speed of the distance feedback rather than the signal-to-noise ratio given by Eq. (16).

E. Time response

In AM-AFM, the time response of the distance feedback is limited by the time constant (τ_{AM}) of the transient response of ΔA to the force changes, which is given by $\tau_{AM} = 2Q/f_0$ (Ref. 2). Thus, AM-AFM has a large disadvantage in high-speed imaging especially in air and vacuum.

In FM-AFM, it has been postulated that the time constant (τ_{FM}) of the transient response of Δf to the force changes is given by $\tau_{FM} = 1/f_0$ (Ref. 2). However, τ_{FM} is practically often slower than this prediction due to the delay caused by the self-excitation circuit (i.e., phase feedback loop).¹⁷ This delay is particularly prominent when a PLL circuit, of which the bandwidth is typically less than 1 kHz, is involved in the self-excitation. In addition, self-excitation is easily disrupted by tip crash or adhesion and, hence, the imaging speed has to be much slower than expected from τ_{FM} .

In PM-AFM, a change in F_{ts} instantaneously results in a change in $\Delta\varphi$. Thus, the time constant (τ_{PM}) of the transient response of $\Delta\varphi$ to the force changes is given by $\tau_{PM} = 1/f_0$, which is faster than τ_{AM} and τ_{FM} . Furthermore, the external excitation of the cantilever enables stable imaging even with occasional tip crash or adhesion to the surface. These features make PM-AFM more suitable for high-speed imaging than AM- and FM-AFMs.

III. EXPERIMENTAL RESULTS

A. Experimental setup

Figure 1 shows the experimental setup for the developed PM-AFM. The cantilever is oscillated with an adjacent piezoactuator driven by an alternating current signal generated with a direct digital synthesizer (DDS). The cantilever deflection is detected with an optical beam deflection sensor and filtered with a bandpass filter. The obtained deflection signal is fed into a lock-in amplifier, where $\Delta\varphi$ is detected. The phase signal is routed to the feedback electronics which control the high voltage signal applied to a tube scanner and thereby regulates the tip-sample separation. Detailed design

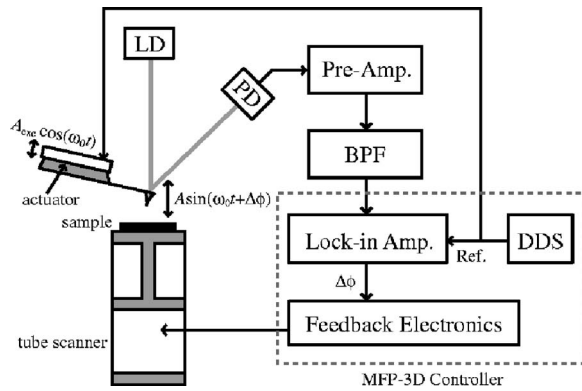


FIG. 1. Schematic drawing of the experimental setup for the developed PM-AFM. The lock-in amplifier, DDS, and feedback electronics are integrated in the AFM controller (Asylum Research: MFP-3D controller).

and performance of the deflection sensor are reported previously.^{13,14} The lock-in amplifier, DDS, and feedback electronics are integrated in a commercially available AFM controller (Asylum Research: MFP-3D controller) and adapted for PM-AFM by modifying the control software.

B. Phase noise

Figure 2 shows phase noise spectra of a cantilever oscillation driven by external excitation measured in water with various oscillation amplitudes. The figure shows that the experimentally measured values (solid lines) agree well with the theoretically calculated values with Eq. (12) (dotted lines) for a wide range of oscillation amplitudes ($A=0.39-7.7$ nm). This demonstrates that n_{zs} is negligible compared to n_{zB} . Thus, the developed PM-AFM has theoretically limited noise performance.

C. Phase shift versus distance curve

Figure 3 shows examples of $\Delta\phi$ and A versus distance curves measured on mica in water. The $\Delta\phi$ versus distance curve shows a typical force profile between two surfaces: an

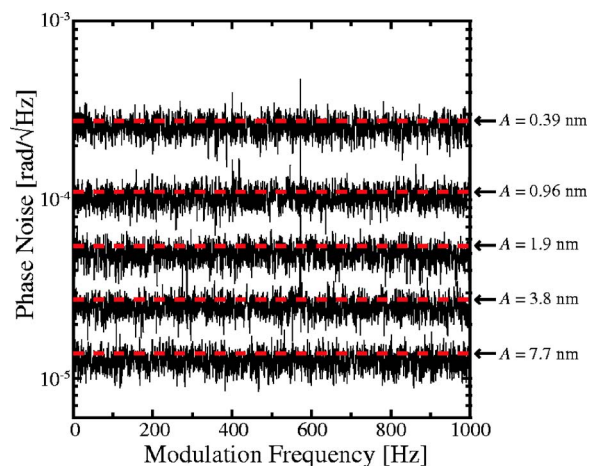


FIG. 2. (Color online) Phase noise density spectra of a cantilever oscillation driven by external excitation measured in water with various oscillation amplitudes ($A=0.39-7.7$ nm). The solid lines show experimentally measured values while the dotted lines indicated by the arrows correspond to the theoretically calculated values with Eq. (12). A Si cantilever (Nanosensors: NCH) with $k=18.8$ N/m, $f_0=142.858$ kHz, and $Q=5.8$ was used.

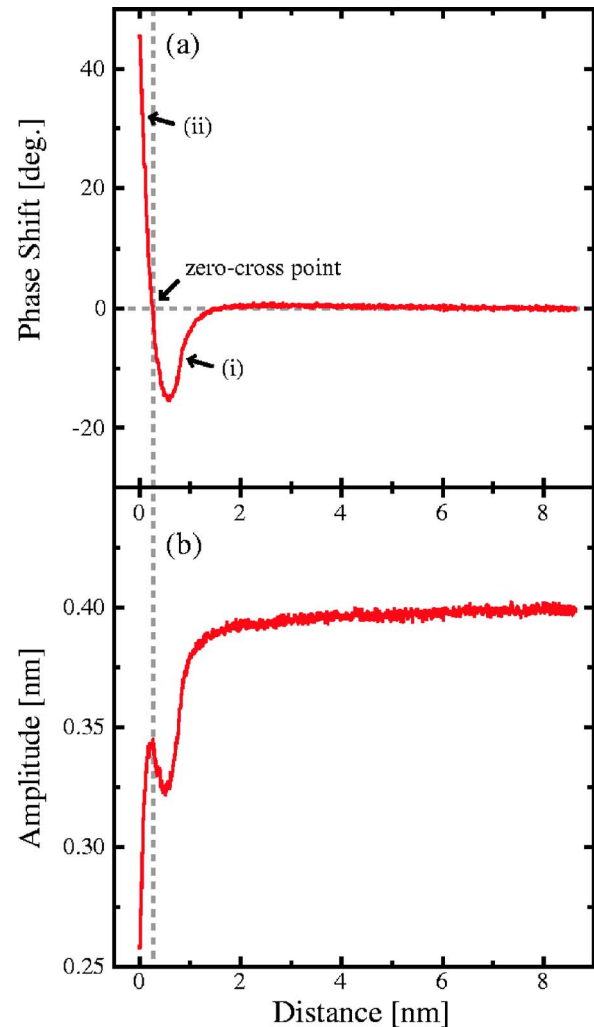


FIG. 3. (Color online) (a) $\Delta\phi$ and (b) A vs distance curves measured on mica in water. A Si cantilever (Nanosensors: NCH) with $k=24.9$ N/m, $f_0=143.238$ kHz, and $Q=6.2$ was used.

attractive force regime and subsequent repulsive force regime as the tip approaches the surface. This is consistent with the expectation from Eq. (6) that $\Delta\phi$ is directly related to the conservative force.

The A versus distance curve shows a small peak at a distance corresponding to the zero-cross point of the $\Delta\phi$ versus distance curve, indicated by an arrow. As the tip approaches the surface, an attractive force starts to induce a negative shift of the resonance frequency, which results in a slight decrease in A . Continuing the tip approach causes a positive shift of the resonance frequency due to an increase of the repulsive force contribution. This results in a transient increase and subsequent decrease of A , which appears to be a small peak in A versus distance curve.

The tip-sample distance feedback can be operated either on branch (i) or branch (ii) indicated in Fig. 3(a). In liquid, the force profile is not necessarily the same as the one shown in Fig. 3, which may restrict the use of branch (i). For example, branch (i) is often small or nonexistent due to a small attractive force.²² In vacuum, the distance feedback has to be operated with a small $\Delta\phi$ setpoint to meet the condition given by Eq. (18). Thus, the setpoint has to be adjusted to a

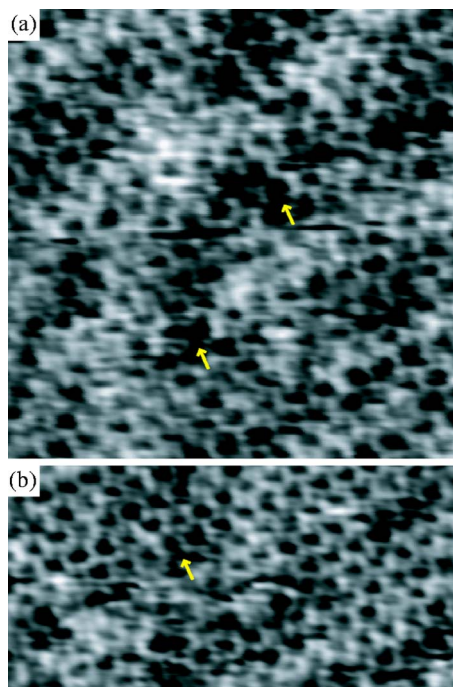


FIG. 4. (Color online) PM-AFM images of mica obtained in water. (a) $7.5 \text{ nm} \times 7.5 \text{ nm}$, $454 \text{ pixels} \times 227 \text{ lines}$, $\Delta\phi = +6.8^\circ$, $A = 0.59 \text{ nm}$, tip velocity: 469 nm/s . (b) $9 \text{ nm} \times 4.5 \text{ nm}$, $378 \text{ pixels} \times 378 \text{ lines}$, $\Delta\phi = +6.8^\circ$, $A = 0.59 \text{ nm}$, tip velocity: 469 nm/s . A Si cantilever (Nanosensors: NCH) with $k = 18.8 \text{ N/m}$, $f_0 = 142.858 \text{ kHz}$ and $Q = 5.8$ was used.

value around the zero-cross point indicated by the arrow in Fig. 3(a).

The slope of the $\Delta\phi$ versus distance curve at the zero-cross point was $\partial\Delta\phi/\partial z = 100 \text{ deg/nm}$ while the experimentally measured phase noise density was $n_p = 0.01 \text{ deg}/\sqrt{\text{Hz}}$. Thus, the z distance resolution with $B = 1 \text{ kHz}$ is about 3.2 pm . This resolution is high enough to resolve atomic-scale corrugation whose height is typically $10\text{--}100 \text{ pm}$ (Ref. 18).

D. Imaging mica in water

Figure 4 show PM-AFM images of mica obtained in water. The images show a honeycomb-like pattern which is characteristic of the atomic-scale structure of a cleaved mica surface.^{14,23} In particular, the top left part of Fig. 4(b) shows atomic-scale protrusions along the honeycomb lattice which have been previously attributed to Al^{+3} ions.²³ Furthermore, the images show atomic-scale defects as indicated by arrows.

These irregular atomic-scale features demonstrate the true-atomic resolution of the developed PM-AFM.

The tip velocity during the imaging was 469 nm/s , which is relatively fast for high-resolution imaging. The imaging speed of the developed PM-AFM is not limited by the signal-to-noise ratio but by the time response of the piezo-tube scanner in our current system. Thus, the imaging speed may be further improved by replacing the scanner with a more rigid one with a higher resonance frequency.

ACKNOWLEDGMENTS

This research was supported by Science Foundation Ireland Research Grant Nos. 01/PI.2/C033 and 00/PI.1/C028.

- ¹Y. Martin, C. C. Williams, and H. K. Wickramasinghe, *J. Appl. Phys.* **61**, 4723 (1987).
- ²T. R. Albrecht, P. Grütter, D. Horne, and D. Ruger, *J. Appl. Phys.* **69**, 668 (1991).
- ³Q. Zhong, D. Inniss, K. Kjoller, and V. B. Elings, *Surf. Sci.* **290**, L688 (1993).
- ⁴T. Fukuma, K. Kobayashi, T. Horiuchi, H. Yamada, and K. Matsushige, *Jpn. J. Appl. Phys., Part 1* **39**, 3830 (2000).
- ⁵T. Fukuma, K. Kobayashi, T. Horiuchi, H. Yamada, and K. Matsushige, *Thin Solid Films* **397**, 133 (2001).
- ⁶F. J. Giessibl, *Science* **267**, 68 (1995).
- ⁷S. Kitamura and M. Iwatsuki, *Jpn. J. Appl. Phys., Part 2* **34**, L1086 (1995).
- ⁸B. Gotsmann, C. Seidel, B. Anczykowski, and H. Fuchs, *Phys. Rev. B* **60**, 11051 (1999).
- ⁹M. Guggisberg *et al.*, *Phys. Rev. B* **61**, 11151 (2000).
- ¹⁰U. Dürig, *New J. Phys.* **2**, 5 (2000).
- ¹¹H. Hölscher, B. Gotsmann, W. Allers, U. D. Schwarz, H. Fuchs, and R. Wiesendanger, *Phys. Rev. B* **64**, 075402 (2001).
- ¹²J. E. Sader, T. Uchihashi, M. J. Higgins, A. Farrell, Y. Nakayama, and S. P. Jarvis, *Nanotechnology* **16**, S94 (2005).
- ¹³T. Fukuma, M. Kimura, K. Kobayashi, K. Matsushige, and H. Yamada, *Rev. Sci. Instrum.* **76**, 053704 (2005a).
- ¹⁴T. Fukuma and S. P. Jarvis, *Rev. Sci. Instrum.* **77**, 043701 (2006).
- ¹⁵A. Engel, Y. Lyubchenko, and D. Müller, *Trends Cell Biol.* **9**, 77 (1999).
- ¹⁶J. Tamayo, A. D. L. Humphris, and M. J. Miles, *Appl. Phys. Lett.* **77**, 582 (2000).
- ¹⁷U. Dürig, H. R. Steinauer, and N. Blanc, *J. Appl. Phys.* **82**, 3641 (1997).
- ¹⁸*Noncontact Atomic Force Microscopy (Nanoscience and Technology)*, edited by S. Morita, R. Wiesendanger, and E. Meyer (Springer, New York, 2002).
- ¹⁹F. J. Giessibl, H. Bielefeldt, S. Hembacher, and J. Mannhart, *Appl. Surf. Sci.* **140**, 352 (1999).
- ²⁰F. J. Giessibl, *Appl. Phys. Lett.* **76**, 1470 (2000).
- ²¹F. J. Giessibl, S. Hembacher, H. Bielefeldt, and J. Mannhart, *Science* **289**, 422 (2000).
- ²²T. Fukuma, K. Kobayashi, K. Matsushige, and H. Yamada, *Appl. Phys. Lett.* **86**, 193108 (2005).
- ²³T. Fukuma, K. Kobayashi, K. Matsushige, and H. Yamada, *Appl. Phys. Lett.* **87**, 034101 (2005).